Dynamic Nonlinear Analysis of Stiffened Shell Structures

보강된 쉘구조의 동적 비선형해석

최 명 수*   김 문 영**   장 승 필***

Choi, Myeong Su   Kim, Moon Young   Chang, Sung Pil

국문요약

보강된 판 및 쉘구조의 동적 비선형해석을 수행하기 위하여, 유한회전을 고려한 변형된 쉘유한요소를 이용하여 total Lagrangian formulation이 제시된다. 전단구속 (shear locking) 현상과 가상의 제로에너지 모우드를 동시에 제거하기 위하여 가정변형도 개념을 채용한다. 탄소성해석에서는 return mapping algorithm이 쉘구조의 붕괴 해석에 적용된다. Newmark 직접적분법을 사용하여 동하중 및 지진하중을 받는 쉘구조의 동적 비선형해석 결과를 제시한다.

주요어 : 동적해석, 쉘구조, 기하학적 비선형, 탄소성해석, 가정변형도 쉘요소

ABSTRACT

For the dynamic nonlinear analysis of stiffened plate and shell structures, total Lagrangian formulation is presented based upon the degenerated shell element considering finite rotation effects. Assumed strain concept is adopted in order to overcome shear locking phenomena and to eliminate spurious zero energy mode. In the elasto-plastic analysis, the return mapping algorithm based on the consistent elasto-plastic tangent modulus is applied to collapse analysis of shell structures. Newmark integration method is used for dynamic nonlinear analysis of shell structures under dynamic forces.

Key words : dynamic analysis, shell structure, geometric non-linearity, return mapping algorithm, assumed strain shell element

1. Introduction

A degenerate shell element which is easily applicable to plate and shell analysis was first presented by Ahmad, Irons and Zienkiewicz.[1] This element was derived from a three dimensional element by applying a so-called degeneration process. The classical Krichhoff hypothesis was no longer fulfilled since out-of-plane shear strains were taken into account. This element and its numerous versions have been used for both linear and nonlinear problems. However, these elements suffer from shear locking and membrane locking.

To overcome these phenomena, a number of authors have developed elements based on the "assumed strain" concept. MacNeal[2] used an assumed strain concept to develop a 4-node element and 6-node triangular element. Huang and Hinton[3] and Huang[4] have proposed elements based on the use of assumed covariant transverse shear strains referred to element natural coordinates, for membrane strains used a local Cartesian coordinate system to separate bending and membrane strains and mixed interpolated only the membrane part. Bathe and Dvorikin[5] and Bucalem and Bathe[6] presented the elements based on the mixed interpolation of tensorial components approach for 9-node and 16-node shell element.

In the development of structural elements for the post-buckling analysis, the consideration of large rotations introduces additional difficulties due to the non-vectorial nature of finite rotations. In the conventional nonlinear formulation for degenerate shell elements, the tangent stiffness matrix is derived by assuming infinitesimal rotation increments and the effect of large rotation increments is considered only during the equilibrium iterations when calculating the stresses. The kinematics of large rotation was studied extensively by Argyris[8] and formulations that take into account the effect of finite rotation increments on the resulting stiffness have been presented by Surana.[9]

In this study, the element formulation is based on the degenerate shell element and the assumed strain concept is adopted. In the elasto-plastic analysis, the return mapping algorithm[11] is applied to the anisotropic shell structures. A finite element formulation accounting the second order effects of finite rotations is presented in order to analyze the geometric nonlinear and elasto-plastic behaviors of stiffened plate and shell structures. Finally Newmark method is used for dynamic nonlinear analysis of shell structures.

2. A total Lagrangian formulation of degenerated shell element considering large rotations

2.1 Effect of finite rotations

The position vector of any point inside the shell element at time t can be expressed as,

$$^{t}X_{i} = \sum_{k=1}^{n} N_{k}{}^{t}X_{i}^{k} + \frac{t}{2}\sum_{k=1}^{n} N_{k}h_{k}{}^{t}V_{3i}^{k} \tag{1}$$

where N_{k} is the element shape function at node k, h_{k} is the shell thickness, and $^{t}V_{3i}^{k}$ is a 'normal' vector at time t.

The incremental displacement from the configuration at time t to the configuration at time $t + \Delta t$ is defined as,

$$\overline{U}_{i} = {}^{t+\Delta t}X_{i} - {}^{t}X_{i} = \sum_{k=1}^{n} N_{k}U_{i}^{k} + \frac{t}{2}\sum_{k=1}^{n} N_{k}h_{k}({}^{t+\Delta t}V_{3i}^{k} - {}^{t}V_{3i}^{k}) \tag{2}$$

The changes in the direction cosines of the normal can be expressed as

$$^{t+\Delta t}V_{3}^{k} - {}^{t}V_{3}^{k} = -{}^{t}V_{2}^{k}\theta_{1}^{k} + {}^{t}V_{1}^{k}\theta_{2}^{k} - \frac{1}{2}{}^{t}V_{3}^{k}(\theta_{1}^{k2} + \theta_{2}^{k2}) \tag{3}$$

By substituting Eq. (3) into Eq. (2), the resulting incremental displacement of any point inside the shell element can be expressed by two terms,

$$\overline{U}_{i} = U_{i} + U_{i}^{*} \tag{4}$$

where U_{i} is the incremental displacement obtained by considering only infinitesimal rotation increments(standard linearization), and U_{i}^{*} is the extra term due to the quadratic terms in the incremental displacement.

Hence,

$$U_{i} = \sum_{k=1}^{n} N_{k}U_{i}^{k} + \frac{t}{2}\sum_{k=1}^{n} N_{k}h_{k}(-{}^{t}V_{2i}^{k}\theta_{1}^{k} + {}^{t}V_{1i}^{k}\theta_{2}^{k}) \tag{5}$$

and

$$U_{i}^{*} = \frac{t}{2}\sum_{k=1}^{n} N_{k}\frac{h_{k}}{2}[-{}^{t}V_{3i}^{k}(\theta_{1}^{k2} + \theta_{2}^{k2})] \tag{6}$$

In the usual formulation, the linear and nonlinear strain-displacement transformation matrices used in the total Lagrangian formulation may be obtained from Eq. (1) to Eq. (6), except for the second order terms. However for more accurate evaluation of the element geometric stiffness of structural elements, the second order terms with respect to the generalized rotational degree of freedom should be added to the nonlinear strain terms of the incremental equations.

2.2 Incremental equilibrium equations

Virtual work principle for the general continuum is expressed as(Bathe, 1996),

$$\int_{V} {}^{t+\Delta t}_{0}S_{ij} \cdot \delta({}^{t+\Delta t}_{0}\varepsilon_{ij})^{0}dV = {}^{t+\Delta t}R = \int_{S} {}^{t+\Delta t}T_{i}\delta^{t+\Delta t}U_{i}{}^{0}dS \tag{7}$$

where

$$^{t+\Delta t}_{0}\varepsilon_{ij} = \frac{1}{2}({}^{t+\Delta t}_{0}U_{i,j} + {}^{t+\Delta t}_{0}U_{j,i} + {}^{t+\Delta t}_{0}U_{k,i}{}^{t+\Delta t}_{0}U_{k,j}) \tag{8}$$

and $^{t+\Delta t}_{0}S_{ij}$ and $^{t+\Delta t}_{0}\varepsilon_{ij}$ are the second Piola-Kirchhoff stress and the Green-Lagrange strain at time $t + \Delta t$ referred to the configuration at time 0, respectively. The incremental displacement components at time t and $t + \Delta t$ are

$$^{t+\Delta t}U_{i} = {}^{t}U_{i} + U_{i} + U_{i}^{*} \tag{9}$$

where U_{i} denotes the first order terms of the displacement parameters and U_{i}^{*} denotes the second order terms due to large rotations, and their sum consists of incremental displacement. Substituting Eq. (9) into Eq. (8) and neglecting higher order terms, the incremental equation of strains is expressed as

$$_{0}\varepsilon_{ij} = {}^{t+\Delta t}_{0}\varepsilon_{ij} - {}^{t}_{0}\varepsilon_{ij} = {}_{0}e_{ij} + {}_{0}\eta_{ij} + {}_{0}e_{ij}^{*} \tag{10}$$

where

$$_{0}e_{ij} = \frac{1}{2}({}_{0}U_{i,j} + {}_{0}U_{j,i} + {}^{t}_{0}U_{k,i}{}_{0}U_{k,j} + {}_{0}U_{k,i}{}^{t}_{0}U_{k,j})$$

$$_{0}\eta_{ij} = \frac{1}{2}{}_{0}U_{k,i}{}_{0}U_{k,j}$$

$$_{0}e_{ij}^{*} = \frac{1}{2}({}_{0}U_{i,j}^{*} + {}_{0}U_{j,i}^{*} + {}^{t}_{0}U_{k,i}{}_{0}U_{k,j}^{*} + {}_{0}U_{k,i}^{*}{}^{t}_{0}U_{k,j}) \tag{11}$$

The $_{0}e_{ij}$ and $_{0}\eta_{ij}$ are the conventional linear and nonlinear Green-Lagrange strain increment, respectively, and $_{0}e_{ij}^{*}$ is the linear strain increment due to U_{i}^{*}. The incremental equations of equilibrium for a general continuum in the total Lagrangian formulation is expressed as

$$\int_{V}({}_{0}C_{ijkl}{}_{0}e_{kl}\delta e_{ij} + {}^{t}_{0}S_{ij}\delta_{0}\eta_{ij} + {}^{t}_{0}S_{ij}\delta e_{ij}^{*})dV$$

$$= {}^{t+\Delta t}R - \int_{V} {}^{t}_{0}S_{ij}\delta_{0}e_{ij}{}^{0}dV \tag{12}$$

where the first term gives the element elastic stiffness and the last term the element nodal force, whereas the geometric

stiffness results from the contribution of nonlinear strains, i.e. the second and third terms.

2.3 Assumed strain finite element

According to Mindlin-type theories, the rotations are independent of the displacements in both plates and shells. When the finite element method is used in conjunction with Mindlin-type formulations, the shear strain energy predicted by the finite element analysis can be magnified unreasonably even though the average value of the shear strains over the area tends to zero. An artificial method for the elimination of shear and membrane locking is to interpolate new strain fields, so called 'assumed strain field', from the strain values at the sampling points which are appropriately located in individual elements. A number of authors have developed elements based on the 'assumed strain' concept. Among these studies, Huang and Hinton[3] have proposed elements based on the use of assumed covariant transverse shear strains referred to element natural coordinate systems, for membrane strains used a local Cartesian coordinate system to separate bending and membrane strains and mixed interpolated only the membrane part, consequently two distinct coordinate systems are required and some complicated routine is produced. Bucalem and Bathe[6] presented the elements based on the mixed interpolation of tensorial components(covariant strain terms) approach for 9-node and 16-node shell element.

Assumed strain approach adopted in this study is similar to Bathe's method.[6] Assumed covariant strain field is used to define new strain field and interpolated these strain values to the nine Gauss points from the sampling points (Fig. 1). After interpolation, all strain terms are transformed to local coordinate system to calculate physical strains and the membrane strains are extracted from bending strains after transformation. The stiffness matrix terms, associated with shear and membrane strains, are replaced by new strain terms.

2.4 Modeling of stiffener element

In the general shell element, five degrees of freedom are specified at each nodal point. But in the stiffened plate and shell element or in the thin-walled structures where the elements are connected with finite angle, six degrees of freedom are required at the connection nodes.

In this study, all nodal points have five degree of freedom except the connection points connecting the main elements and stiffener elements. In the connection nodes, the rotational degrees of freedom of the stiffener element are referred to that of main shell elements. Therefore coordinate transformation is required only for the stiffener element, and no transformation is needed for the main shell element.

3. Elasto-plastic analysis of shell structures

3.1 Stress-strain relations

The elastic constitutive relation for anisotropic material[10] is used with an assumption that the reference system of orthogonal axes is parallel to the principal material axis. The generalized Von-Mises yield criterion is employed to consider the anisotropic materials. The consistent elasto-plastic tangent moduli(Simo and Taylor[11], 1986) is applied to anisotropic shell element, to define the relationship between the incremental stress and strain.

The basic equations in elasto-plastic problems may be summarized as follows
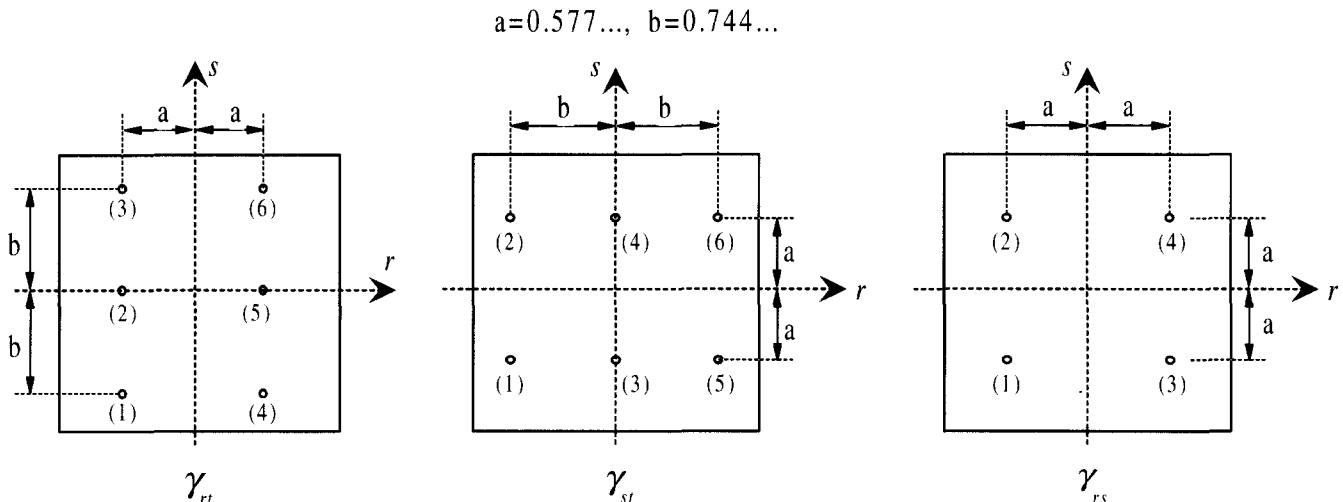
$$a=0.577..., \quad b=0.744...$$

Fig. 1 Sampling points for the 9-node Lagrangian element

1) incremental strain : $d\boldsymbol{\varepsilon} = d\boldsymbol{\varepsilon}^e + d\boldsymbol{\varepsilon}^p$

2) elastic stress-strain relation : $\boldsymbol{\sigma} = \mathbf{D}\boldsymbol{\varepsilon}^e$

3) flow rule : $d\boldsymbol{\varepsilon}^p = d\lambda \mathbf{A}\boldsymbol{\sigma}$

4) yield function : $\Psi = \frac{1}{2}\boldsymbol{\sigma}^T\mathbf{A}\boldsymbol{\sigma} - \frac{1}{3}\sigma_Y^2\left(\bar{e}^p\right) = 0$ (13)

where $\mathbf{A}$ and $\mathbf{D}$ are the anisotropic parameter and elasticity matrix for anisotropic materials (Hinton and Owen[10]), respectively.

The plastic strains $^{t+\Delta t}\boldsymbol{\varepsilon}^p$ and $^{t+\Delta t}\bar{e}^p$ are determined by integration of the flow rule and hardening law over the time step from t to $t+\Delta t$ and the 'generalized midpoint rule' is used to integrate the flow rule. The detailed procedure deriving consistent elasto-plastic tangent muduli based on Return mapping algorithm may be refered to (10).

3.2 Update algorithm

In the general material nonlinear analysis by Newton-Raphson iteration method, the iteration process can be divided into two parts. First is calculating the trial stress using linearized tangential stiffness which corresponds to the elastic predictor. Second is calculating exact stress state with the appropriate yield condition which corresponds to the plastic corrector. In the elastic predictor phase, the quadratic convergence rate can be obtained by using the consistent elasto-plastic tangent modulus rather than classical elasto-plastic tangent modulus. Furthermore, the accuracy of the solution can be obtained by using the return mapping algorithm in the plastic corrector phase. The second part of the algorithm defines a relaxation process towards the yield surface often referred as return mapping.[11]

4. Nonlinear dynamic analysis of shell structures

4.1 Newmark method for dynamic nonlinear analysis

The time integration schemes for linear dynamic analysis can also be employed in nonlinear dynamic response calculations. For using Newmark method, the equilibrium equations at time $t+\Delta t$ can be rewritten as

$$\mathbf{M}^{t+\Delta t}\ddot{\mathbf{U}} + \mathbf{C}^{t+\Delta t}\dot{\mathbf{U}} + {}^{t+\Delta t}\mathbf{K}^{t+\Delta t}\mathbf{U} = {}^{t+\Delta t}\mathbf{R} \qquad (14a)$$

where $\mathbf{C}$ is the Rayleigh damping matrix represented as

$$\mathbf{C} = \alpha\mathbf{M} + \beta^0\mathbf{K} \qquad (14b)$$

This requires in nonlinear analysis that iteration step should be performed. Using the modified Newton-Raphson iteration,

$$\mathbf{M}^{t+\Delta t}\ddot{\mathbf{U}} + \mathbf{C}^{t+\Delta t}\dot{\mathbf{U}} + {}^t\mathbf{K}\Delta\mathbf{U}^{(i)} = {}^{t+\Delta t}\mathbf{R} - {}^{t+\Delta t}\mathbf{F}^{(i-1)} \qquad (15)$$

and

$$^{t+\Delta t}\mathbf{U}^{(i)} = {}^{t+\Delta t}\mathbf{U}^{(i-1)} + \Delta\mathbf{U}^{(i)} \qquad (16)$$

where $^{t+\Delta t}\mathbf{F}^{(i-1)}$ are the element internal forces at the previous iteration step.

In the Newmark integration method, acceleration and velocity vectors are assumed as

$$^{t+\Delta t}\ddot{\mathbf{U}} = a_0\left(^{t+\Delta t}\mathbf{U} - {}^t\mathbf{U}\right) - a_2{}^t\dot{\mathbf{U}} - a_3{}^t\ddot{\mathbf{U}}$$

$$^{t+\Delta t}\dot{\mathbf{U}} = a_1\left(^{t+\Delta t}\mathbf{U} - {}^t\mathbf{U}\right) - a_4{}^t\dot{\mathbf{U}} - a_5{}^t\ddot{\mathbf{U}} \qquad (17)$$

where a_i are the integration constants defined as

$$a_0 = \frac{1}{\alpha\Delta t^2} \qquad a_1 = \frac{\delta}{\alpha\Delta t}$$

$$a_2 = \frac{1}{\alpha\Delta t} \qquad a_3 = \frac{1}{2\alpha} - 1$$

$$a_4 = \frac{\delta}{\alpha} - 1 \qquad a_5 = \frac{\Delta t}{2}\left(\frac{\delta}{\alpha} - 2\right) \qquad (18)$$

Substituting (17) into (15), following equations are obtained for the first iteration step.

$$^t\tilde{\mathbf{K}}\Delta\mathbf{U}^{(0)} = {}^{t+\Delta t}\tilde{\mathbf{R}}^{(0)} \qquad (19)$$

and

$$^t\tilde{\mathbf{K}} = {}^t\mathbf{K} + a_0\mathbf{M} + a_1\mathbf{C}$$

$$^{t+\Delta t}\tilde{\mathbf{R}}^{(0)} = {}^{t+\Delta t}\mathbf{R} + \mathbf{M}\left(a_2{}^t\dot{\mathbf{U}} + a_3{}^t\ddot{\mathbf{U}}\right) + \mathbf{C}\left(a_4{}^t\dot{\mathbf{U}} + a_5{}^t\ddot{\mathbf{U}}\right) - {}^t\mathbf{F}$$

$$(20)$$

For the next iteration steps, effective loads are replaced by effective unbalance loads $^{t+\Delta t}\tilde{\mathbf{R}}^{(i)}$ defined as

$$^{t+\Delta t}\tilde{\mathbf{R}}^{(i)} = {}^{t+\Delta t}\mathbf{R} - \mathbf{M}^{t+\Delta t}\ddot{\mathbf{U}}^{(i)} - \mathbf{C}^{t+\Delta t}\dot{\mathbf{U}}^{(i)} - {}^{t+\Delta t}\mathbf{F}^{(i)} \qquad (21)$$

and the incremental equilibrium equations are

$$^t\tilde{\mathbf{K}}\Delta\mathbf{U}^{(i)} = {}^{t+\Delta t}\tilde{\mathbf{R}}^{(i)} \qquad (22)$$

Then, accelerations and velocities at time $t+\Delta t$ can be obtained as

$$^{t+\Delta t}\ddot{\mathbf{U}}^{(i)} = a_0\Delta\mathbf{U} - a_2{}^t\dot{\mathbf{U}} - a_3{}^t\ddot{\mathbf{U}}$$

$$^{t+\Delta t}\dot{\mathbf{U}}^{(i)} = a_1\Delta\mathbf{U} - a_4{}^t\dot{\mathbf{U}} - a_5{}^t\ddot{\mathbf{U}} \qquad (23)$$

and the total increment of displacements are calculated as (16).

4.2 Dynamic analysis considering effects of support acceleration

Dynamic stresses and deflections can be induced in a structure not only by a time-varying applied load, but also by motion of its support points. Important examples of such excitation are the motions of a structure foundation caused by an earthquake or motions of a equipment due to vibrations of the building in which it is housed.

If the effect of support excitations is included, the dynamic equilibrium equations in (14) can be rewritten as, at time $t + \Delta t$.

$$\mathbf{M}^{t+\Delta t}\ddot{\mathbf{U}}_t + \mathbf{C}^{t+\Delta t}\dot{\mathbf{U}} + \mathbf{K}^{t+\Delta t}\mathbf{U} = {}^{t+\Delta t}\mathbf{R} \qquad (24)$$

and

$$^{t+\Delta t}\ddot{\mathbf{U}}_t = {}^{t+\Delta t}\ddot{\mathbf{U}} + {}^{t+\Delta t}\ddot{\mathbf{U}}_g \qquad (25)$$

where $^{t+\Delta t}\ddot{\mathbf{U}}_t$ represents the total accelerations of the mass from the fixed reference axis and $^{t+\Delta t}\ddot{\mathbf{U}}_g$ the accelerations by the support motion.

In general, the support motion is applied in a specific direction. If the support motion is applied in x-direction, the component of acceleration vector for node i, $^{t+\Delta t}\ddot{\mathbf{U}}^i_g$, can be constructed as

$$^{t+\Delta t}\ddot{\mathbf{U}}^i_g = \begin{bmatrix} 1 \\ 0 \\ 0 \\ 0 \\ 0 \end{bmatrix} {}^{t+\Delta t}\ddot{u}_g \qquad (26)$$

where $^{t+\Delta t}\ddot{u}_g$ is the ground acceleration at time $t + \Delta t$.

The dynamic equilibrium equation (24) can be rewritten as

$$\mathbf{M}^{t+\Delta t}\ddot{\mathbf{U}} + \mathbf{C}^{t+\Delta t}\dot{\mathbf{U}} + \mathbf{K}^{t+\Delta t}\mathbf{U} = {}^{t+\Delta t}\mathbf{R} - \mathbf{M}^{t+\Delta t}\ddot{\mathbf{U}}_g = {}^{t+\Delta t}\mathbf{R}_{eff} \qquad (27)$$

Thus, the inertial forces caused by ground acceleration, $^{t+\Delta t}\ddot{u}_g$, can be treated a the external forces. Therefore, replacing the load vector $^{t+\Delta t}\mathbf{R}$ in (14) by $^{t+\Delta t}\mathbf{R}_{eff}$ in (27), linear and dynamic analysis including the effect of support acceleration can be performed.

5. Numerical examples

For nonlinear analysis, the iterative Newton-Raphson method is applied within admissible maximum iteration until the following convergence condition is satisfied.

$$\left| {}^{t+\Delta t}\lambda^{(i)}\mathbf{P} - {}^{t+\Delta t}\mathbf{F}^{(i)} \right| \leq 100 \cdot Toler \cdot \left| {}^{t}\lambda\mathbf{P} \right| \qquad (28)$$

whereis *Toler* the convergence tolerance given by the input value and 0.1 is used in examples of this study.

5.1 Square plate subjected to suddenly applied load

A simply supported square plate with side-length $L =10$ in, thickness $h =0.5$ in and material density $\rho =0.259 \times 10^{-3}$ lb·sec^2/in^4. is subjected to a suddenly applied uniformly distributed load of 300 psi. The material properties of this example are :

$$E = 1.0 \times 10^7 \text{ psi}$$
$$\nu = 0.3$$
$$G = 38.462 \times 10^5 \text{ psi}$$
$$\sigma_y = 30000 \text{ psi}$$
$$H' = 0.0$$

In the time stepping solution, the time increment adopted is 0.223×10^{-4} s which is $\frac{1}{48}$ of the fundamental period of the plate. A symmetric quadrant of the plate is modeled using a 4×4 mesh.

Fig. 2 compares the central displacement time histories when different through-thickness integration schemes are used. And Table 1 shows the total iteration numbers during 60 time steps. The amplitudes and the periods of the vibration increase with the number of integration points of layers adopted through the plate thickness. As
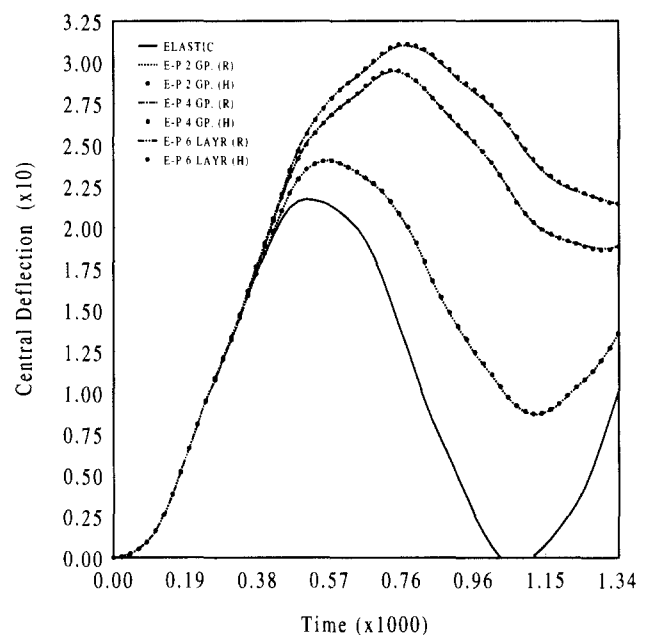

Fig. 2 Time history of central displacement for suddenly applied square plate

Table 1 Total iteration number during 60 time steps2

2 Gauss point		4 Gauss point		6 Layer	
Classical method(H)	Present study(R)	Classical method(H)	Present study(R)	Classical method(H)	Present study(R)
100	82	133	87	136	95

more Gauss points or layers through the thickness of a structure are used, the results become more realistic. (H) and (R) denote the Huang's results[12] and the results from present study using return mapping algorithm, respectively. Resultantly Fig. 2 and Table 1 show that the present results are quite close to the Huang's results, but the iteration numbers to get the solution are considerably decreased by using the return mapping algorithm.

5.2 Free vibration and dynamic analysis of cylindrical shell

Free vibration analysis is performed for a circular cylinder shell structure with vertical stiffeners or horizontal stiffeners and without stiffeners. The cylinder is modeled with 16×8 9-node shell element with radius $R=50$m, height $H=200$m, and thickness $t=0.5$m. The vertical stiffeners are modeled with 8×1 shell element and the horizontal stiffeners are modeled with 16×1 shell element with width $W=5$m and thickness $t=0.5$m for both vertical and horizontal stiffeners. In all cases, the boundaries in the cylinder bottom surface are fixed for translations and rotations. The material properties used for cylinder and stiffeners are as follows :
$E=2.1 \times 10^7 \text{tonf/m}^2$, $\nu =0.3$, $\rho =0.8\text{tonf} \cdot \text{sec}^2/\text{m}^4$

Fig. 3 shows the shell models for each case. The natural frequencies and corresponding mode shapes are given in Table 2 and Fig. 4, respectively. In Table 2 the analysis results of present study are compared with the results from ABAQUS, where the cylinder is modeled with 32×16 8-node shell element and the vertical and horizontal stiffeners are modeled with 16×1 and 32×1 shell element, respectively. As shown in Table 2 and Fig. 4, the natural frequencies of the cylinder with horizontal stiffeners are increased as the stiffness of the structures is increased due to the stiffeners. But the natural frequencies of the cylinder with vertical stiffeners are decreased since the vertical stiffener is not available for increasing the stiffness in radial direction, only increasing the mass of the cylinder.

Fig. 5 shows the analysis results for El Centro earthquake load. As shown in Fig. 5 the responses of the stiffened cylinders are larger than the response of the cylinder without stiffener.
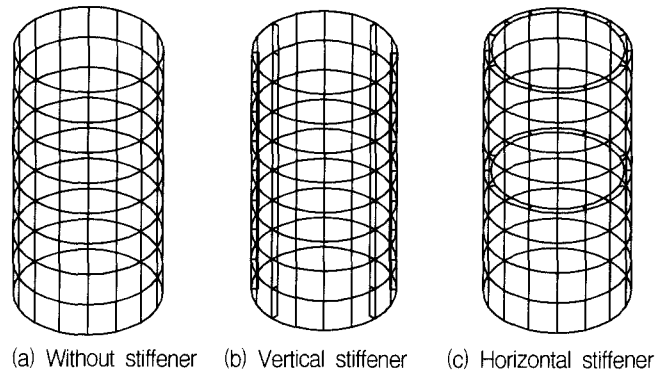

(a) Without stiffener   (b) Vertical stiffener   (c) Horizontal stiffener

Fig. 3 Cylinder shells with vertical and horizontal stiffeners

Table 2 Natural frequencies for cylinder shell

Mode Number	Without stiffener (cycle/sec)		Vertical stiffener (cycle/sec)		Horizontal stiffener (cycle/sec)	
	Present study	ABAQUS	Present study	ABAQUS	Present Study	ABAQUS
1	0.536	0.526	0.508	0.498	0.966	0.934
2	0.536	0.526	0.508	0.498	0.966	0.934
3	0.747	0.743	0.704	0.680	1.776	1.740
4	0.747	0.743	0.723	0.718	1.776	1.740
5	0.783	0.755	0.723	0.718	1.789	1.770

Mode 1

Mode 2

Mode 3

Mode 4

Mode 5

(a) Without stiffener   (b) With vertical stiffener   (c) With horizontal stiffener
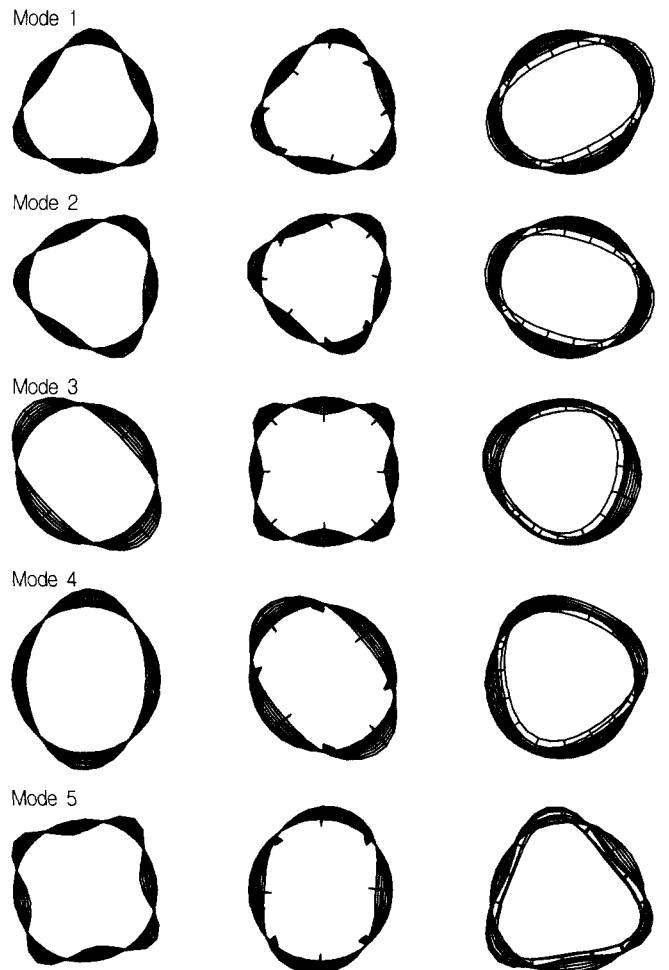
Fig. 4 First 5 mode shapes for cylindrical shell
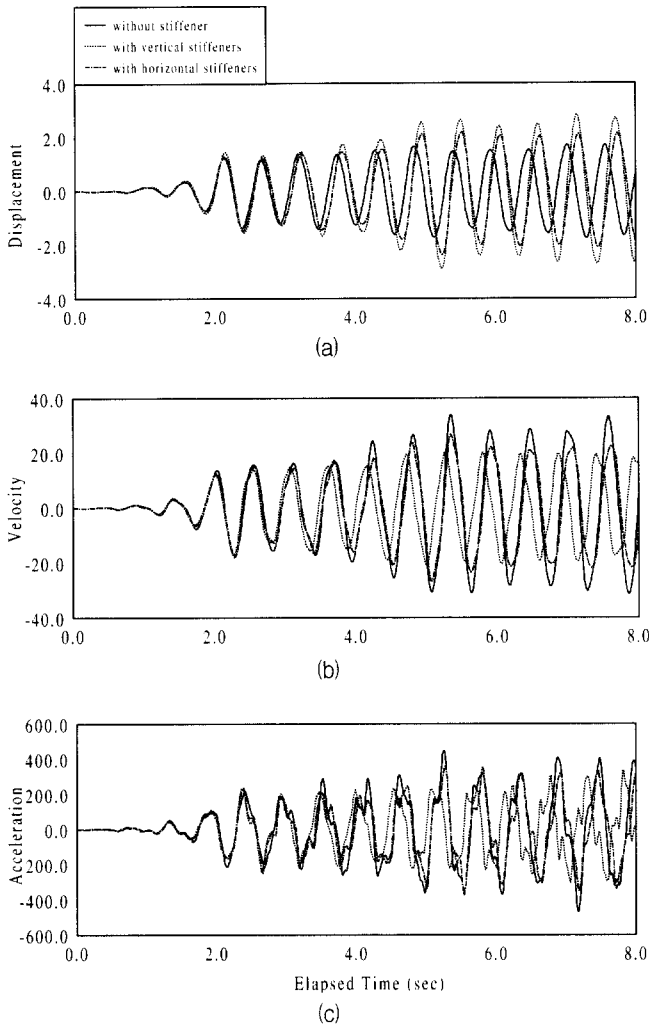
Fig. 5 Response of cylinder shell under earthquake load

Fig. 6 Undeformed and deformed shape of cantilever plate

(a) Lateral displacements   (b) Axial displacements
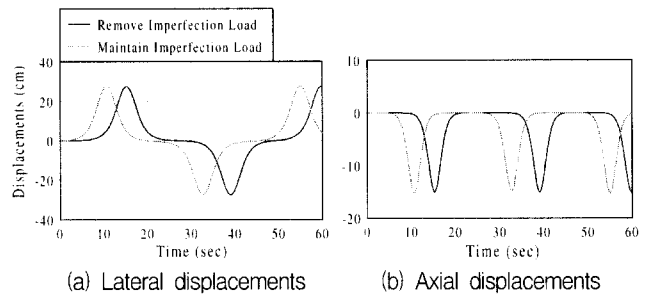
Fig. 7 Post-divergence behavior without damping

(a) $\alpha=0.1$ $\beta=0.0$ (b) $\alpha=0.2$ $\beta=0.0$

(c) $\alpha=0.3$ $\beta=0.0$ (d) $\alpha=0.4$ $\beta=0.0$
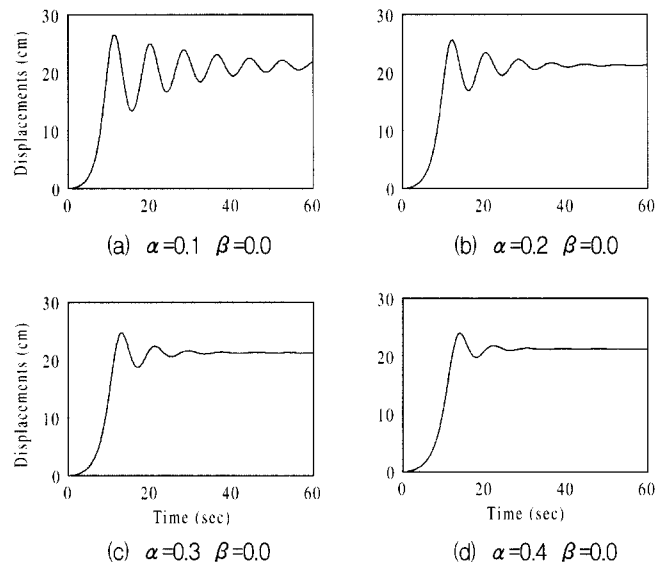
Fig. 8 Post-divergence behavior with various damping ratio

5.3 Dynamic buckling of cantilever plate

A simple cantilever plate with length L=40cm, height H=4cm, thickness t=0.5cm and material density ρ =0.8kgf·sec^2/cm^4 is analyzed for suddenly applied axial load to investigate dynamic buckling behavior. Fig. 6 shows the undeformed and deformed shapes of cantilever plate for maximum and minimum displacements of cantilever tip end, resulted from the dynamic buckling behavior for a suddenly applied axial load of 1.5KN slightly larger than the static buckling load(1.35KN) of the cantilever. Fig. 7 shows the lateral displacements of the free end without damping and Fig. 8 shows the same results for various damping ratios. As shown in Fig. 7, if there is no damping force lateral displacement of free end is oscillating with an amplitude 27.4cm. If there is a damping force, lateral displacement of free end is converged to the lateral displacement 21.2cm for a static loading of 1.5KN, as shown in Fig. 8. The lateral displacement is more rapidly converged to the static displacement as the damping ratio is larger, as expected.
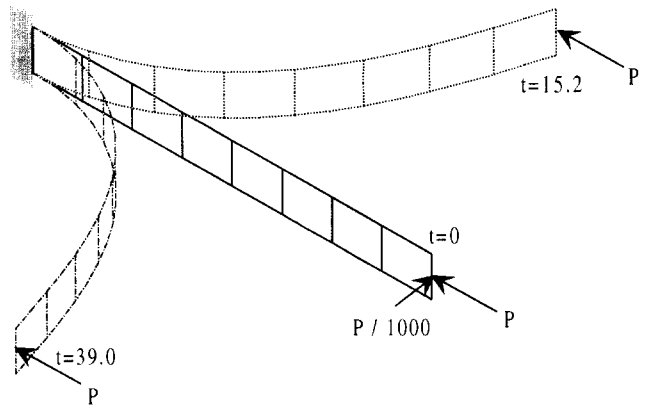
6. Conclusion

In this study the ultimate strength analysis, including the large deformation and elasto-plastic analysis of shell structures is preformed using the degenerate shell element. The assumed strain concept is adopted to overcome locking phenomena, which is the main defect of the displacement based isoparametric finite element especially for thin shell situation, and to eliminate the spurious zero energy modes occurring when reduced or selective integration methods are used. In geometric nonlinear analysis, more exact solutions

are obtained by evaluating the total Green-Lagrangian strains corresponding to total displacements and by including the effect of second order rotation terms in the incremental displacement field. In the elasto-plastic analysis, the return mapping algorithm is applied to the anisotropic shell structures. Through numerical examples, it is demonstrated that the elasto-plastic behavior of thin plates under dynamic loadings is effectively traced using Return mapping algorithm and also, dynamic buckling behaviors of the damped cantilever plate are accurately obtained under the suddenly applied end load.

References

1. Ahmad, S., Irons, B. M., and Zienkiewicz, O. C., "Analysis of thick and thin shell structures by curved element," *Int. J. Numer. Methods Eng.*, Vol. 2, 1970, pp. 419-451.
2. MacNeal, R. H., "Derivation of element stiffness matrices by assumed strain distributions," *Nuclear Engineering Des.*, Vol. 70, 1982, pp. 2-12.
3. Huang, H. C. and Hinton, E., "A new nine node degenerated shell element with enhanced membrane and shear interpolation," *Int. J. Numer. Methods Eng.*, Vol. 22, 1986, pp. 73-92.
4. Huang, H. C., "Implementation of assumed strain degenerated shell elements," *Computers and Structures*, 25, 1987, pp. 147-155.
5. Bathe, K. J. and Dvorikin, E. N., "A four-node plate bending element based on Mindlin/Reissner plate theory and a mixed interpolation," *Int. J. Numer. Methods Eng.*, 21, 1985, pp. 367-383.
6. Bucalem, M. L. and Bathe, K. J., "Higher-order MITC general shell elements," *Int. J. Numer. Methods Eng.*, Vol. 36, 1993, pp. 3729-3754.
7. Bathe, K. J., *Finite Element Procedures in Engineering Analysis*, Prentice-Hall, 1996.
8. Argyris, J., "An excursion into large rotations," *Comp. Methods in Appl. Mech. and Engrg*, Vol. 32, 1982, pp. 85-155.
9. Surana, K. S., "Geometrically nonlinear formulation for the curved shell elements," *Int. J. Numer. Methods Eng.*, Vol. 19, 1983, pp. 581-615.
10. Hinton, E. and Owen, D. R. J., *Finite Element Software for Plates and Shells*, Pineridge Press, 1985.
11. Simo, J. C. and Taylor, R. L., "A return mapping algorithm for plane stress elastoplasticity," *Int. J. Numer. Methods Eng.*, Vol. 22, 1986, pp. 649-670.
12. Huang, H. C., *Static and Dynamic Analyses of Plates and Shells*, Springer-Verlag, Berlin, 1989.
13. Choi, M. S., "Ultimate Strength Analysis of Stiffened Shell Structures," Ph. D. Thesis, Seoul National University, 1999.